Catalytic system, based on recyclable Fe^0 and ZnS semiconductor for UV-promoted degradation of chlorinated organic compounds

Olga Sacco[1], Vincenzo Vaiano[2], Wanda Navarra[1], Christophe Daniel[1], Stefania Pragliola[1], Vincenzo Venditto[1]**

(1) Department of Chemistry and Biology "A. Zambelli", and INSTM Research Unit, University of Salerno, Via Giovanni Paolo II, 132, 84084 Fisciano (SA), Italy

(2) Department of Industrial Engineering, and INSTM Research Unit, University of Salerno, Via Giovanni Paolo II 132, 84084 Fisciano (SA), Italy

* Corresponding authors:

E-mail: vvaiano@unisa.it; Tel: +39/089964340

E-mail vvenditto@unisa.it; Tel: +39/089969589

ABSTRACT

Fe^0 (ZVI) is one of the most effective reactants for treatment of water contaminated with chlorinated hydrocarbons, pollutants recalcitrant to degradation. Unfortunately, ZVI use is limited by corrosion and loss of reactivity over time. In order to suppress oxidation and passivation phenomena of iron, in this study ZVI was coupled to a suitable semiconductor (ZnS). Under UV light, electrons in the valence band of ZnS are promoted in the conducting band (E_{CB} = −1.04 eV vs NHE) and are able to reduce Fe^{2+} to Fe^0 (E_0 = −0.44 eV vs NHE). The ZnS_ZVI composite was simply prepared by coating commercial ZnS with Fe^0 obtained by reducing Fe (II) salt with sodium borohydride. The achieved ZnS_ZVI catalytic system was

characterized by FESEM, WAXD, Raman and N_2 adsorption at -196 °C, with the aim to analyze morphology and crystalline structure of both components of the ZnS_ZVI system. Catalytic activity tests showed that ZnS_ZVI is effective in degrading probe molecules, eriochrome black T dye (EBT) and chlorobenzene (PhCl), from aqueous solutions under UV light irradiation. The experimental results show that in both cases the reductive action of Fe^0 on the N=N bond of EBT and C-Cl of PhCl is synergistically coupled to the oxidative action of ZnS towards by-products. OH radicals, generated by the reaction between the electron holes in the valence band of ZnS and H_2O (OH^-), were indeed confirmed by photoluminescence analysis. Recyclability tests indicate that ZnS_ZVI is highly stable since its catalytic activity, on both probe molecules, remains unchanged even after several cycles of reuse under UV irradiation. ZnS_ZVI catalytic behavior towards EBT has been carefully analyzed and a possible mechanism of EBT degradation has been proposed, which involves the formation of a Fe^{2+}-EBT complex whose structure has also been suggested.

KEYWORDS: zero-valent iron; ZnS; chlorobenzene; eriochrome black T-dye; UV light

1. Introduction

The increasing accumulation of toxic organic/inorganic pollutants in water streams and groundwater natural reservoirs represents a pressing worldwide problem [1]. Particularly relevant is the concern for pollutants recalcitrant to degradation. Among them, chlorinated hydrocarbons are typically treated in aqueous media with Fe^0 (ZVI) which reacts with halogenated pollutants (RX) and H^+ according to the following general reaction [2-5]:

$$Fe^0 + RX + H^+ = Fe^{2+} + RH + X^-$$

The above reaction involves the ZVI oxidation and the pH increase, which in turn promotes the formation of iron hydroxides, which are deposited on the ZVI surface by passivating it and reducing its reactivity [2]. Corrosion and loss of reactivity limit ZVI use in long-term engineering processes for the remediation of groundwater, such as in permeable reactive barriers. To overcome corrosion phenomena, recently, the ZVI surface modification by deposition of small amounts of a second metal with high positive redox potential (such as Pd, Pt, Ag, Ni and Cu) led to an increase of ZVI performances[6-8]. However, a loss of activity over time was observed, due to accumulation of metal oxides or chemisorption of other compounds onto active sites or loss of the weakly bound second metal particles, making the benefit of bimetals only short-lived [6, 9]. In order to enhance the ZVI performances, some authors recently proposed to add TiO_2 or ZnO semiconductor photocatalysts to ZVI with the aim of coupling the photocatalytic degradation action of semiconductors together with the reductive action of ZVI [10-13]. Furthermore, ZVI was also recently added to g–C_3N_4 and g–C_3N_4/MoS_2 with the aim to promote the photogenerated electron−hole pairs separation and improve the photocatalytic efficiency [14, 15].

Inspired by these recent articles, we considered the idea of coupling ZVI to a semiconductor

which, if properly irradiated, would provide electrons to reduce Fe^{2+} to Fe^0. Therefore, in order to identify a suitable candidate among the most used semiconductors in photocatalysis [16-27], the valence band (VB) edge potential (E_{VB}) of the ground-state together with conduction band (CB) edge potential (E_{CB}) of several semiconductors (reported in Table S1 of Supplementary Material) were considered and compared to Fe^{2+}/Fe^0 reduction potential (E_0=−0.44 eV vs. NHE) [24, 28, 29]. Among the considered semiconductors, ZnS was selected as its band-gap energy (see Table S1 of Supplementary Material), E_{VB} and E_{CB} values are equal to 3.6, 2.56 and −1.04 eV vs. NHE, respectively [24, 25]. Based on these data, when ZVI is coupled with ZnS and the system is UV light irradiated, the photoexcited electrons in the ZnS CB (E_{CB}=−1.04 eV vs. NHE) could reduce Fe^{2+} into Fe^0 (E_0=−0.44 eV vs. NHE). Moreover, the holes created in the ZnS VB could react with OH^- (coming from H_2O dissociation) to form OH radicals [30], since the E_{VB} of ZnS (+2.56 eV vs. NHE) is more positive than the potential of $E^{\cdot}_{OH/OH-}$ (+1.99 eV vs. NHE).

Based on these considerations, ZnS was coupled with ZVI by a facile procedure to obtain a ZVI/ZnS composite (ZnS_ZVI). The effectiveness of regeneration and reusability of ZnS_ZVI catalytic system was tested in the degradation of two target molecules, an azo dye (eriochrome black T-dye) and a chlorinated organic compound (chlorobenzene) from aqueous solutions under UV light irradiation. Furthermore, a possible mechanism of EBT degradation was proposed, which involves the formation of a Fe^{2+}-EBT complex, whose structure has also been suggested, and the action of hydroxyl radicals generated by the ZnS semiconductor, the presence of which has also been detected by experimental tests with terephthalic acid as a chemical probe.

It is worth noting that, to the best of our knowledge, no specific studies aimed at maintaining the efficiency of ZVI in water pollutant removal by continuous regeneration of the zero oxidation state of iron under UV light irradiation, have been reported in literature. It is also worth noting

93 that the ZVI coupling with the ZnS semiconductor, reported in this paper, has never been
94 previously described in literature.

95 **2. Materials and methods**

96 *2.1 Materials*

97 Zinc sulfide (ZnS), sodium borohydride ($NaBH_4$) and iron (II) sulfate heptahydrate ($FeSO_4$) were
98 purchased from Sigma–Aldrich, while commercial ZVI was purchased from Höganäs (Sweden).
99 Eriochrome black-T and chlorobenzene, used in the catalytic tests as model pollutants, were
100 provided by Sigma-Aldrich.

101 *2.2 Synthesis of ZVI, and ZnS_ZVI using the chemical reduction method*

102 ZVI was synthetized [31] starting from 100 mL of an aqueous solution containing 4 g of $FeSO_4$
103 (S1). As for ZnS_ZVI, 1 g of ZnS was added to the S1 aqueous solution obtaining an aqueous
104 suspension (S2).
105 The solution S1 or the suspension S2 was stirred for 10 min and then, a gaseous He flow (flow
106 rate: 30 $NL \cdot h^{-1}$) was bubbled inside the system in order to remove the oxygen dissolved in the
107 aqueous phase. Afterward, the reducing agent ($NaBH_4$) was added both into S1 solution and S2
108 suspension. The quantity of $NaBH_4$ to be added was evaluated considering an excess of 30%
109 with respect to the stoichiometric ratio pointed out in the following reaction:
110 $Fe^{2+} + BH_4^- + 2\ H_2O = Fe^0 + BO_2^- + 2H^+ + 3H_2$ Eq.1

111 The obtained suspension was left under stirring in presence of He flow for 1 h, washed with
112 distilled water three times and finally dried overnight at room temperature, obtaining ZVI, and
113 ZnS_ZVI samples.

The nominal ZVI loading in ZnS_ZVI catalysts was equal to 45 wt % [32] and it was calculated according to the following relationship (Eq. 2):

$$\%ZVI = \frac{gZVI}{(gZVI + gZnS)} \cdot 100 \qquad \text{Eq.2}$$

Where:

gZVI is the weight of iron calculated from $FeSO_4$ amount in S1 and *gZnS* is the weight of ZnS used in S2 preparation.

2.3. Samples characterization.

The catalysts were characterized by several techniques. In particular, the morphology of the samples was examined using a scanning electron microscope (FESEM, mod. LEO 1525, Carl Zeiss SMT AG, Oberkochen, Germany). Total iron loading in the ZnS_ZVI sample was determined by atomic absorption spectroscopy and inductively coupled plasma-optical emission spectrometry (ICP-OES Optima 7000DV, PerkinElmer). Before the ICP analysis, the sample was mineralized with a hydrochloric acid aqueous solution.

Raman spectra were obtained with a Dispersive MicroRaman spectrometer (Invia, Renishaw) with a 514 nm laser in the range 100-800 cm^{-1}.

Wide-angle X-ray diffraction (WAXD) patterns were performed with an automatic Bruker D8 Advance diffractometer (VANTEC-1 detector) using reflection geometry and nickel filtered Cu-Kα radiation.

The crystallite average sizes (D) were calculated using the Scherrer equation (Eq.3):

$$D = \frac{0.9\,\lambda}{\beta \cos\theta} \qquad \text{Eq. 3}$$

where β is the full width at half-maximum (FWHM) expressed in radians, λ the wavelength, and θ the X-ray diffraction angle.

Finally, the specific surface area (SSA) measurement was performed by BET method using N_2 adsorption at -196 °C with a Costech Sorptometer 1042 after pretreatment at 35°C for 2 hours in He flow (99.9990 %).

2.4 Reactivity tests

The reactivity of the ZnS_ZVI composite was evaluated by removing the Eriochrome black-T dye (EBT) and chlorobenzene (PhCl) from aqueous solutions. The initial concentration of EBT was equal to 100 mg L^{-1} (spontaneous pH of the solution: 4.7), while the initial concentration of PhCl was equal to 50 mg L^{-1} (spontaneous pH of the solution: 6.7). All reactivity tests were carried out, at ambient temperature and pressure, by using 75 mL of pollutant aqueous solutions and a catalyst dosage of 0.6 g L^{-1}. The experiments were conducted in a pyrex cylindrical reactor (ID = 2.6 cm, L= 41 cm and V= 200 mL). The continuous mixing of the suspensions was realized by external recirculation through a peristaltic pump. A thermocouple was inserted inside the reactor to monitor the temperature during UV light irradiation. The tests were performed both in dark and under UV irradiation. The UV light irradiation was obtained by using four UVA lamps (TL8W BLB provided by Philips; UV light intensity at the external surface of the photoreactor: 26 mW cm^{-2}) [33] with main emission wavelength at 365 nm.

During the tests, at regular time intervals, about 2.0 mL of solution were taken from the reactor, centrifuged to remove catalyst particle residues and analyzed by using UV-vis spectrophotometer to detect pollutant concentrations. In detail, the concentrations were measured with a Perkin Elmer UV-vis spectrophotometer (Lambda 35) monitoring the band of EBT and PhCl, at λ=574

157 [34] and 255 nm, respectively [35]. More specifically, for a correct evaluation of the
158 concentration of EBT molecules in solution during the test time, absorbance spectra were
159 acquired in the range 200-700 nm and the curve fitting analysis of the line shapes to set of
160 Gaussian functions was performed using Origin 8.5 software (Figure S1 of Supplementary
161 Material). EBT mineralization during the test time in presence and absence of UV light was
162 analyzed in terms of the total organic carbon (TOC) reduction. TOC of aqueous solution was
163 measured from CO_2 obtained by catalytic combustion at T = 680 °C [36].
164 The ability of ZnS_ZVI sample to generate ·OH under UV light was determined using
165 terephthalic acid (TA) as a chemical probe since TA is converted into 2-hydroxyterephthalic acid
166 (hTA) by chemical reaction with ·OH [37]. In detail, 50 mg of ZnS_ZVI catalyst was added to
167 50 mL of TA solution (5×10^{-4} M) in 2×10^{-3} M NaOH. The suspension was irradiated by UV
168 light (at 365 nm) for 180 min. Before the analysis, the suspension was filtrate through 0.45 μm
169 membrane to separate the photocatalyst from the solution. Then the production of ·OH during
170 irradiation time was evaluated by measuring the fluorescence intensity generated by hTA
171 molecules in water solutions using Duetta Fluorescence and Absorbance Spectrometer (HORIBA
172 Instruments Incorporated) exciting the solution at 315 nm and measuring the fluorescence at 425
173 nm.

174 **3. Results and Discussion**

175 *3.1 ZVI, ZnS and ZVI_ZnS composite characterization*

176 In Figure 1 scanning electron microscope images (SEM) of ZVI prepared by using the procedure
177 described in section 2 (A), commercial ZVI powder (B), ZnS powder (C, D) and ZnS_ZVI (E, F)
178 samples, are reported.

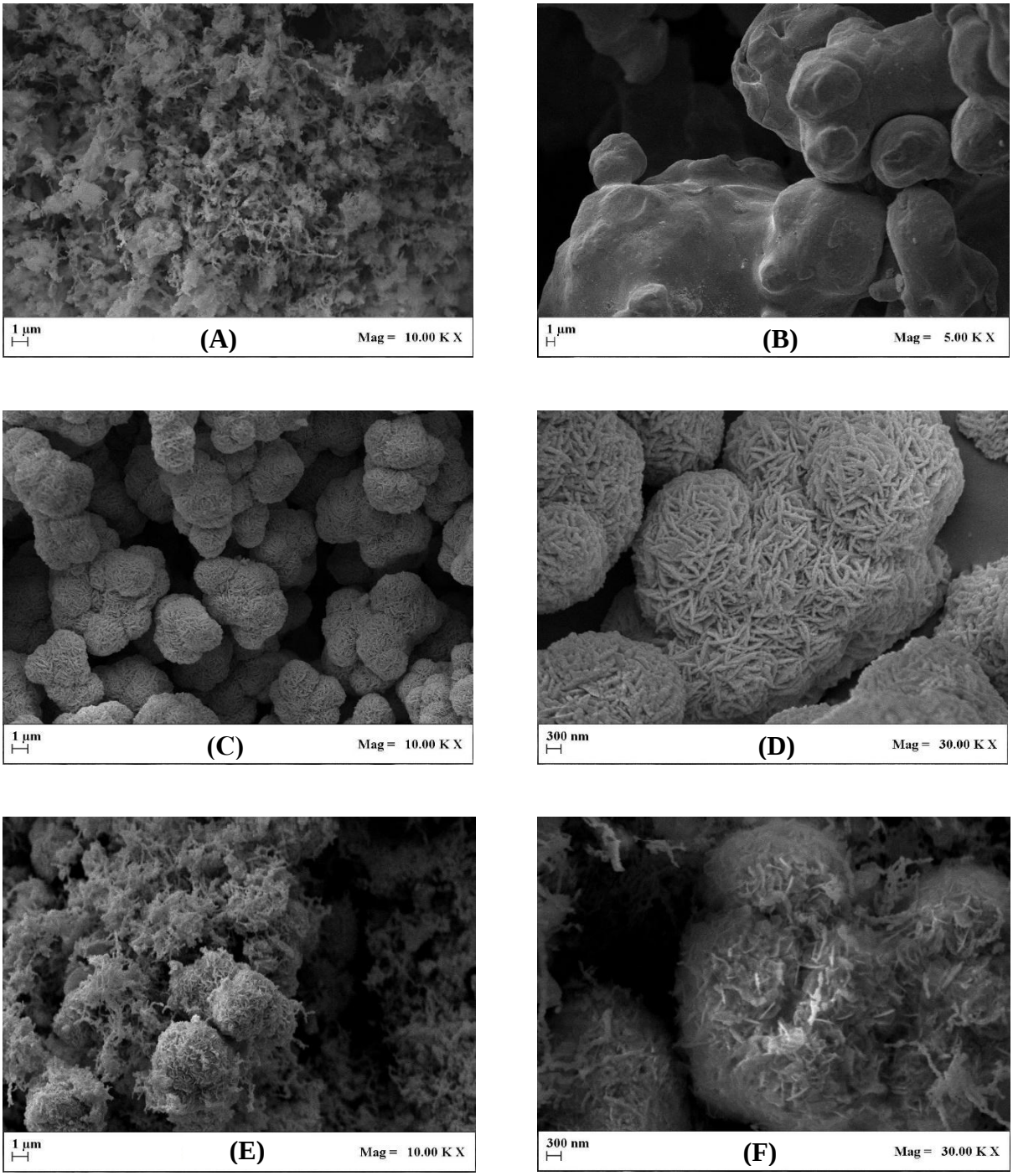

179 **Figure 1**. SEM images of ZVI (A), commercial ZVI powder (B), ZnS powder (C, D), and

180 ZnS_ZVI (E, F) samples.

ZVI, achieved by us, is characterized by a highly developed network structure (Figure 1A) totally different from the compact morphology observed for the commercial ZVI powder (Figure 1B). The SEM images reveal that the native ZnS sample consists of 2-10 μm sphere-like aggregates (Figure 1C) composed of flakes (Figure 1 D). After coupling with ZVI, the aggregate structure of ZnS remain substantially unaltered but an additional inter-penetrated ZVI network is formed both between ZnS aggregates (Figure 1E) and ZnS flakes (Figure 1F).

Table 1. SSA of commercial ZVI, ZVI, ZnS, and ZnS_ZVI samples and average crystallite size of Fe^0 and ZnS

Catalyst	SSA[c] (m^2/g)	crystallite size (nm)
ZVI (commercial)	< 0.1	50[a]
ZVI	38	12[a]
ZnS	14	25[b]
ZnS_ZVI	44	12 (Fe^0) 25 (ZnS)

[a] evaluated by using the FWHM of (110) reflection
[b] evaluated by using the FWHM of (111) reflection
[c] evaluated by using the BET method

The specific surface area (SSA) value of all samples is reported in Table 1. In detail, for ZVI sample prepared by reduction method, the SSA value (38 $m^2 \cdot g^{-1}$) is significantly higher than that of the commercial ZVI (<0.1 $m^2 \cdot g^{-1}$). This result is in agreement with the observed morphological differences between the two ZVI samples (compare Figure 1A and Figure 1B). When ZVI was coupled with ZnS, an increase of SSA is observed with respect to bare ZnS. In detail, the SSA value for the ZnS_ZVI sample is equal to 44 $m^2 \cdot g^{-1}$ while it is 14 $m^2 \cdot g^{-1}$ for the native ZnS sample. This increase in the SSA value can be attributed to the presence of the inter-

200 penetrated ZVI network.

201 WAXD patterns and Raman spectra of ZVI, ZnS and ZnS_ZVI are reported in Figure 2A and

202 2B, respectively.

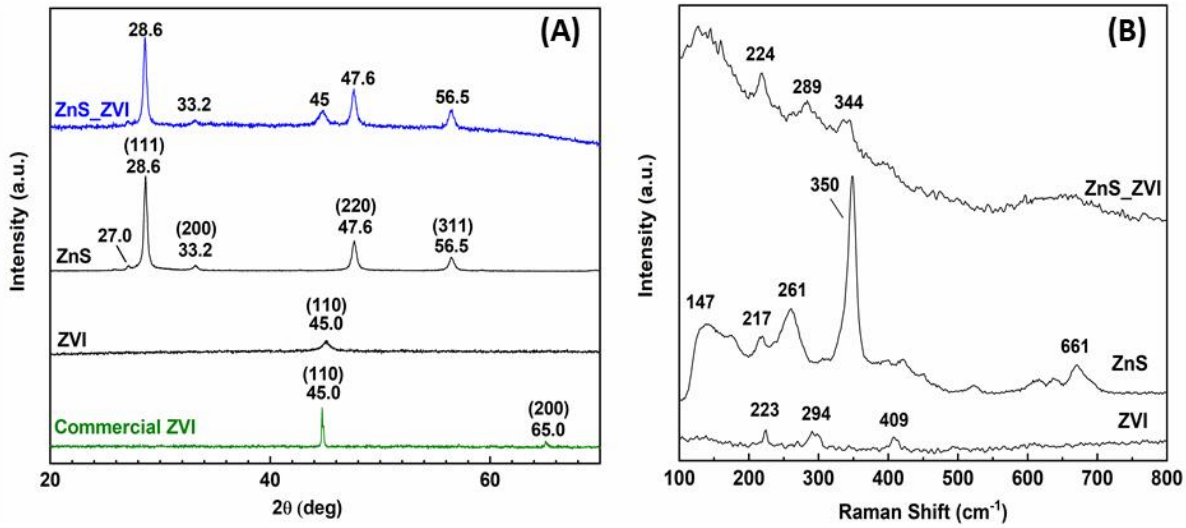

203

204 **Figure 2.** WAXD patterns (A) and Raman spectra (B) of ZVI, ZnS and ZnS_ZVI. For the sake

205 of discussion, the WAXD pattern of commercial ZVI powder is also reported in (A).

206 The WAXD patterns of both commercial ZVI and ZVI achieved by us by chemical reduction of

207 Fe^{2+} in liquid phase display a diffraction peak at c.a. 2θ= 45° corresponding to the (110)

208 reflection of α-Fe body-centered cubic crystal lattice. However, the average crystallite size

209 reported in Table 1, calculated by Scherrer formula using the full width at half maximum

210 (FWHM) of (110) reflection, indicates that ZVI crystallite size is lower than that of commercial

211 ZVI (c.a. 50 nm and 12 nm, respectively). The WAXD pattern of ZnS shows diffraction peaks at

212 28.6, 33.2, 47.6 and 56.5° which can be assigned to the (111), (200), (220) and (311) reflections

213 of the zinc blende phase, respectively [25]. The weak intensity diffraction peak at 2θ= 27°

214 reveals that traces of ZnS wurtzite phase are also present. With respect to the ZnS sample,

ZnS_ZVI composite presents only one additional peak at 45° due to the ZVI (Figure 2B) [38]. The average crystallite size of the cubic ZnS phase in neat ZnS and ZnS_ZVI samples, evaluated by using FWHM of (111) reflection, is approximately constant and equal to 25 nm. It is worth noting that the average crystallite size of ZVI is equal, c.a. 12 nm, in both ZVI and ZnS_ZVI. This result indicates that ZVI crystallites size depends only on ZVI preparation procedure.

The Raman spectrum of ZVI (Figure 2B) displays weak resonant peaks at 223, 294 and 409 cm^{-1} which indicate the formation of a small amount of α-Fe_2O_3, while the Raman spectrum of ZnS powder presents a main peak at 350 cm^{-1}, commonly referred in literature as an LO mode [39], and several weaker peaks at 147, 217, 261 and 671 cm^{-1} typically observed for Raman spectra of ZnS powder collected under green excitation conditions [39]. For the ZnS_ZVI sample, both the α-Fe_2O_3 peaks at 223 and 294 cm^{-1} were observed along with the ZnS LO mode.

Finally, as for the iron amount in the ZnS_ZVI composite, ICP-MS analysis indicates a value of 43.5 wt %, approximately equal to that one calculated in the composite preparation step.

3.2 Degradation of EBT using ZnS and ZnS_ZVI in dark conditions and in presence of UV irradiation

Two preliminary tests were carried out: the first one with an aqueous solution containing EBT dye in the presence of UV light but without catalyst dispersed in the reaction medium and the second one in presence of ZVI alone but without irradiation (Figure S2 in Supplementary Materials). The results evidence that EBT relative concentration does not change under UV light irradiation for 180 min, indicating that the photolysis of EBT molecules can be neglected. On the other hand, for ZVI sample, a noticeably faster decrease of EBT concentration occurs. In detail, the EBT relative concentration decreases after 5 min of treatment to about 76%. However, after a

treatment time of 60 min, the EBT relative concentration remained constant and equal to about 90%.

Figure 3 shows the results of EBT degradation tests using ZnS_ZVI and bare ZnS under UV light irradiation and in dark conditions.

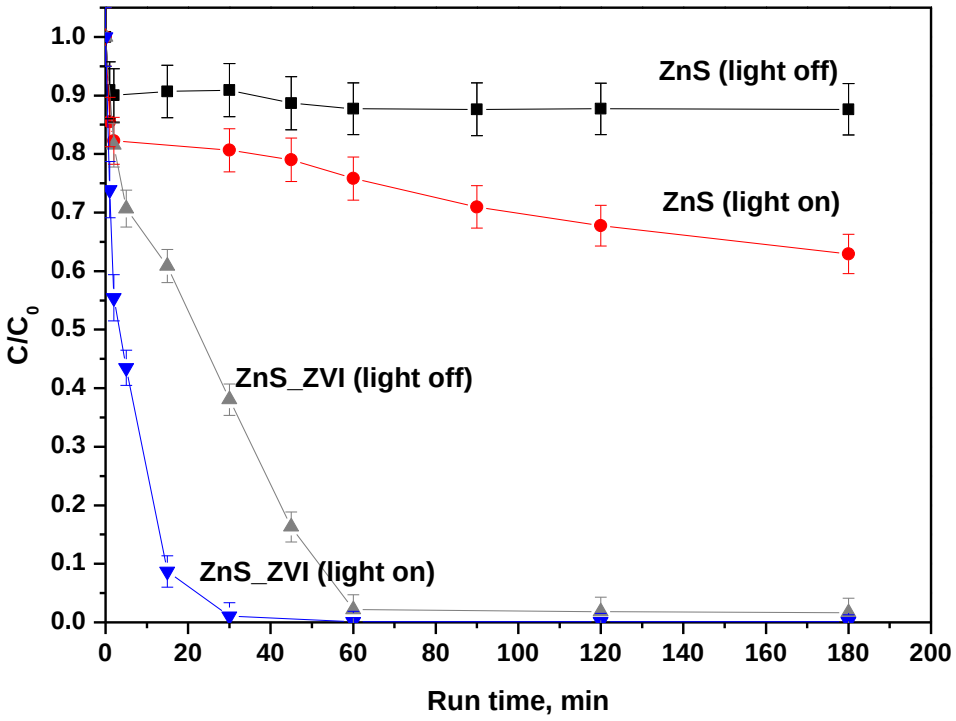

Figure 3. Comparison of EBT degradation efficiencies using ZnS_ZVI and ZnS in dark conditions (light off) and in presence of UV light (light on)

In dark conditions, the bare ZnS does not exhibit any capability to degrade the EBT (the decrease of dye relative concentration in the first 2 minutes is due to the adsorption of EBT molecules on the ZnS surface), whereas, when it is irradiated with UV light, a slow progressive decrease of EBT concentration is observed, and degradation efficiency of about 40% is obtained after 180 min of irradiation.

As for the ZnS_ZVI composite, under UV irradiation the EBT relative concentration decreases very quickly, reaching the almost complete dye degradation after 30 min of irradiation, whereas, after the same time, the non-irradiated composite shows a dye degradation efficiency of only about 60 %. It is worth noting that, under UV irradiation, the EBT degradation efficiency of the ZnS_ZVI composite within 30 min is four times higher than that shown by bare ZnS after 180 min. Figure 4 reports the TOC behavior as a function of run time using ZnS_ZVI under UV light irradiation and in dark conditions. No TOC removal is observed in the absence of UV light, whereas, under irradiation, the ZnS_ZVI composite is also able to promote the mineralization of the target dye, achieving a TOC removal of about 45 % after 180 min of run time.

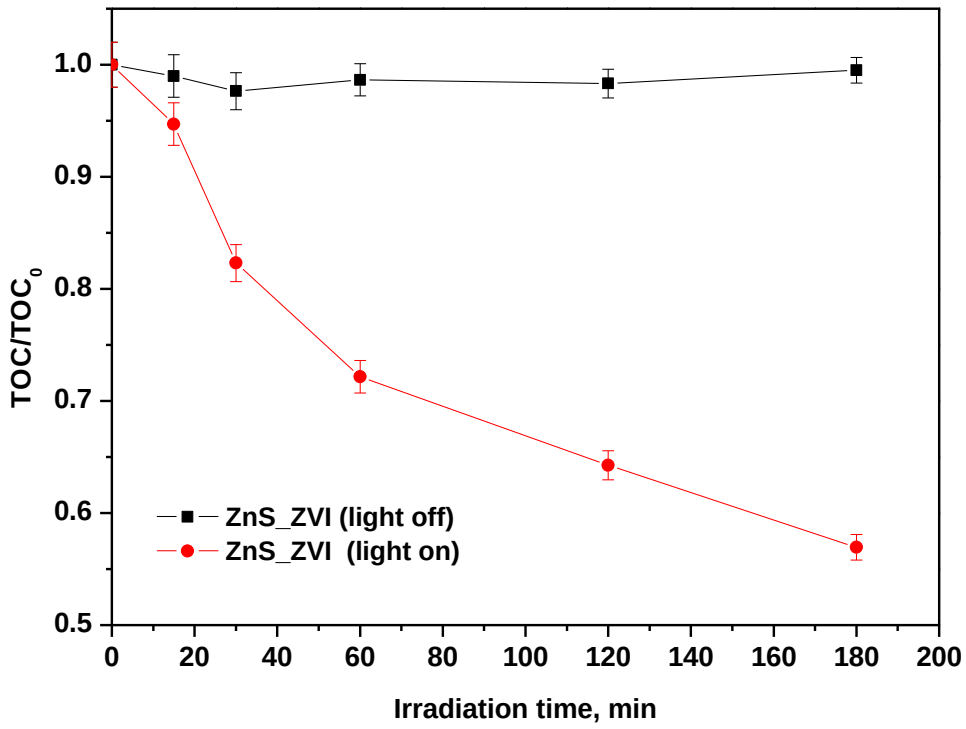

Figure 4. Comparison of mineralization efficiencies using ZnS_ZVI and ZnS in dark conditions (light off) and in presence of UV light (light on).

3.2.1 Reusability of ZnS_ZVI

In order to verify whether the semiconductor/iron coupling was actually able to reduce Fe^{2+} to Fe^{0} and therefore to maintain the system catalytic efficiency over time, tests to evaluate the reuse/recycling efficiency of the composite were conducted. It is worthwhile to note that, no regeneration step of ZnS_ZVI was carried out before reusing it. Specifically, after reacting for 60 min, the catalyst powders were separated from the treated water and dried at room temperature, after which it was dispersed again into a fresh aqueous solution of EBT.

Values of EBT degradation percentage, obtained by using ZnS_ZVI for successive cycles, are shown in Figure 5.

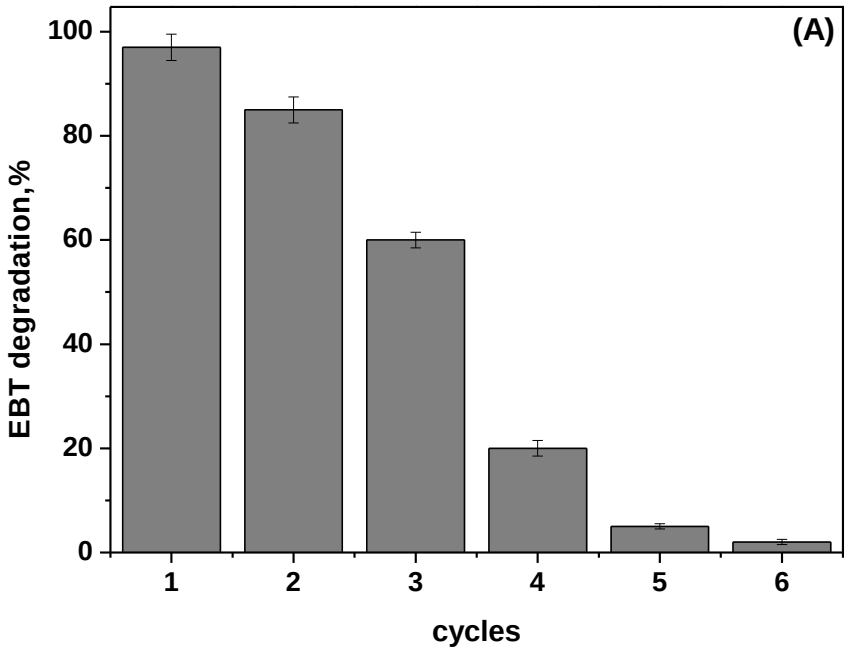

275

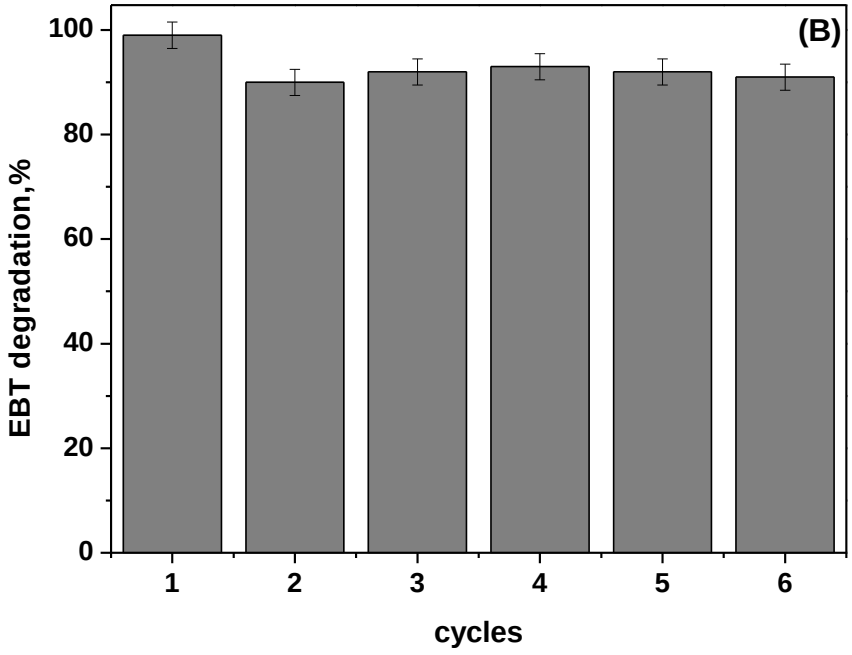

276

277 **Figure 5.** Reuse cycles of ZnS_ZVI without (A) and with UV irradiation (B), after 60 min of

278 treatment time

279 In absence of UV light (Figure 5 A), the percentage of EBT degradation gradually decreases for
280 each cycle, so that after six cycles it is reduced to c.a. 2%. This degradation efficiency decrease
281 is consistent with previous papers reported in literature [11, 40], and can be trivially related to
282 the progressive oxidation of ZVI into Fe^{2+} responsible for the reduction of EBT azo bond
283 (-N=N-). Therefore, the ZVI of ZnS_ZVI composite, in absence of UV light irradiation, is
284 consumed during the EBT degradation reaction and cannot be reused.

285 Different behavior is observed when ZnS_ZVI is irradiated by UV light (Figure 5B). In this case,
286 after an initial negligible reduction of degradation efficiency, the composite maintains a constant
287 reactivity (about 90%), up to the sixth cycle. This behavior can be rationalized by considering a
288 continuous ZVI regeneration process (reduction of Fe^{2+} to Fe^0) by the ZnS semiconductor
289 coupled to it since, under UV light, the photoexcited electrons in the ZnS CB (E_{CB}=−1.04 eV vs.
290 NHE) [24, 25] can effectively reduce Fe^{2+} into Fe^0 (E_0=−0.44 eV vs. NHE) [24, 28, 29], as
291 pointed above.

292 *3.2.2 UV-vis studies and proposed EBT degradation mechanism*

293 The UV–vis spectra of EBT aqueous solutions treated with ZnS_ZVI, UV light irradiated or not,
294 were also analyzed at different treatment times (Figure 6). As shown in Figure 6A, if EBT
295 aqueous solutions is not UV light irradiated, the intensity of absorbance bands in the range 630-
296 700 nm, associated to EBT azo bond (-N=N-), quickly decreases, due to the well-known
297 reductive action of ZVI promoting the azo bond cleavage [41-43]. On the other hand, increasing
298 the treatment time, new absorbance signals at about 320, 435 and 525 nm appear in the UV-vis
299 spectra. Based on literature data [44-46], both the bands at 320 and 435 nm can be associated to
300 substituted aminonaphtalene species containing (435 nm) or not containing (320 nm) a nitro
301 substituent. The appearance of these absorbance bands, associated to substituted

aminonaphtalenes, is reported to be coupled with the appearance of bands at wavelengths below 285 nm, attributed to organic compounds containing primary amino groups ($-NH_2$) [46]. The presence of these bands, even if not clearly detectable, cannot be excluded in Figure 6A.

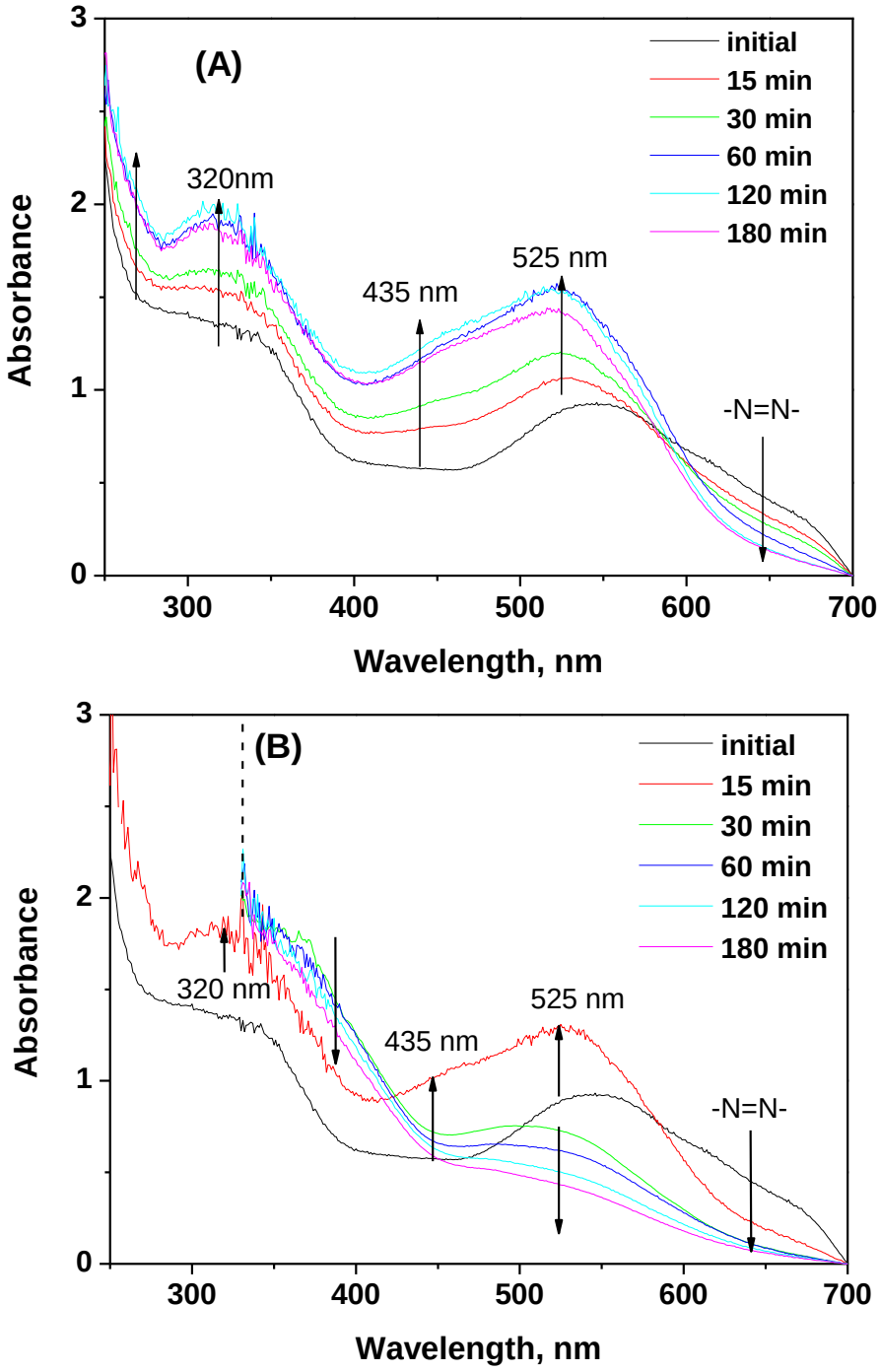

Figure 6. UV-Vis spectra of EBT solutions treated with ZnS_ZVI, without (A) and with UV irradiation (B).

316 On the basis of these UV absorbance band attributions and consistently with reported ZVI
317 promoted azo dye degradation reactions [42, 47] (and also when inorganic pollutants are
318 considered [48]), we hypothesize that the degradation of EBT by ZVI_ZnS occurs by reductive
319 cleavage of the ETB azo bond without destroying naphthalene rings [42, 47], according to the
320 Scheme 1.
321

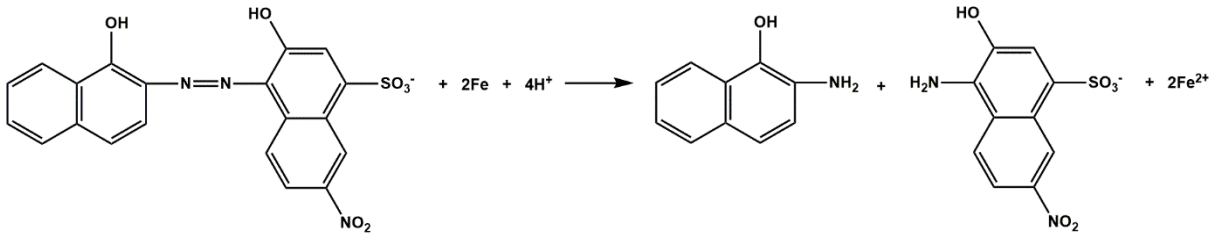

322

323 **Scheme 1.** Degradation of EBT promoted by ZnS_ZVI composite

324 As regards the absorbance band at 525 nm (Figure 5A), it is reported to be associated to metal-
325 to-ligand charge transfer (MLCF) transitions [49]. Therefore, since the ability of Fe^{2+} to form
326 chelate complexes with EBT in aqueous medium is well known [50, 51], this band has been
327 associated to a complex between EBT and Fe^{2+} (Scheme 2).
328

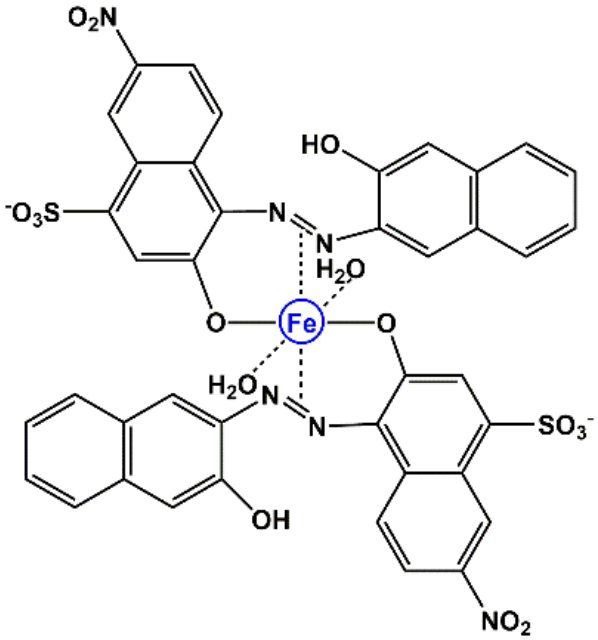

Scheme 2. Fe^{2+}-EBT complex

For this Fe^{2+}-EBT complex, different structures, having octahedral geometry and presenting one [50, 51] or two [49, 52] ETB molecules coordinated to the iron have been proposed. For both these complexes, the metal coordinative sphere is completed by H_2O molecules.

In order to establish how many ETB molecules are involved in the Fe^{2+}-EBT complex formed during the EBT degradation, a simple experiment was set up. Considering that the final pH of the test with EBT in dark condition was 6.9, buffer aqueous solutions (pH = 7, buffer: phosphate) of Fe^{2+} and EBT were prepared using well defined molar ratios EBT/Fe^{2+}. In detail, solutions presenting molar ratios EBT/Fe^{2+} in the range 1/1 to 3/1 were considered and analysed by UV-vis spectroscopy (see Figure S3 in Supplementary Materials). The spectroscopic analysis indicates that the band at 525 nm, associated with the presence of the Fe^{2+}-EBT complex, is the main band detectable until the EBT/Fe^{2+} molar ratio is less than 2/1. Bands in the range 630-700 nm, associated with free EBT molecules, appear only when the EBT/Fe^{2+} molar ratio exceeds 2/1. In detail, the intensity of the band at 525 nm strictly increases linearly as the EBT/Fe^{2+} ratio

344 increases up to 2/1, and remains constant for higher EBT/Fe^{2+} values (see Figure S4 in
345 Supplementary Materials).
346 Based on these results, we concluded the Fe^{2+}-EBT complex structure involves two EBT
347 molecules, as shown in Scheme 2.
348 Figure 6B shows the UV–vis spectra of UV light irradiated EBT aqueous solutions at different
349 treatment times. As observed in the EBT solution treated in absence of UV light irradiation, a
350 very fast decrease of the intensity of absorbance bands in the range 630-700 nm is also observed,
351 in presence of UV light irradiation (Figure 6A). After 15 min of treatment time, the absorbance
352 signals at 320, 435 mm (due to naphthalene rings) and at about 525 nm (associated to Fe^{2+}-EBT
353 complex) already appeared. However, for test time higher than 15 min, the intensity of these
354 absorbance bands progressively decreases under UV light irradiation. This behavior can be
355 interpreted as result of catalytic action of the ZnS, which irradiated by UV light degrades the
356 R–NH_2 (2-Amino-1-naphthol) and R'-NH_2 (6-nitro-1-amino-2-naphthol-4-sulfonate) by-
357 products of EBT azo bond cleavage (Scheme 1), as well as the Fe^{2+}-EBT complex. In detail, the
358 ZnS catalytic action follows the typical and widely reported action mechanism of a
359 semiconductor. Under UV light irradiation, electrons jump from VB to CB of ZnS and holes (h^+)
360 are produced into ZnS VB. The h^+ induces formation of hydroxyl radicals ($OH^{\cdot}$), which oxidize
361 R–NH_2 and R'-NH_2 giving oxidized intermediate products and possibly continue the oxidative
362 degradation action until mineralization [34]. It is worth noting that, generation of $OH^{\cdot}$ by ZnS
363 was confirmed by using terephthalic acid (TA) as chemical probe. TA molecules, in presence of
364 ZnS_ZVI catalyst and under UV light irradation, are converted into 2-hydroxyterephthalic acid
365 (hTA) by chemical reaction with ·OH [37] and the hTA molecules production can be evaluated
366 by measuring the hTA fluorescence intensity. The obtained results (Figure S5 in Supplementary

Material) evidence that hTA fluorescence signal increased under UV irradiation, evidencing the ability of ZnS_ZVI composite in the generation of ·OH in aqueous solution. To support the hypothesis about EBT degradation mechanism by means of ZnS_ZVI composite under UV light, a series of radical capture experiments were performed for identifying and confirming the main involved active species [53, 54]. In detail, the scavenger probe molecules used in the activity tests were: isopropanol (IPA, 10 mmol L^{-1}) for hydroxyl radicals [22], benzoquinone (BQ, 1 μmol L^{-1}) for superoxide [22] and zinc chloride (ZC, 1 mmol L^{-1}) for electrons. ZC was chosen as scavenger for electrons because Zn^{2+}/Zn^{0} reduction potential (E_0=−0.76 eV vs. NHE) is more negative than Fe^{2+}/Fe^{0} reduction potential (E_0=−0.44 eV vs. NHE). In this situation, the electrons promoted in the CB of ZnS preferentially reduce Zn^{2+} into Zn^{0} [55], inhibiting the reduction of Fe^{2+} to Fe^{0}. Figure 7 shows the obtained results.

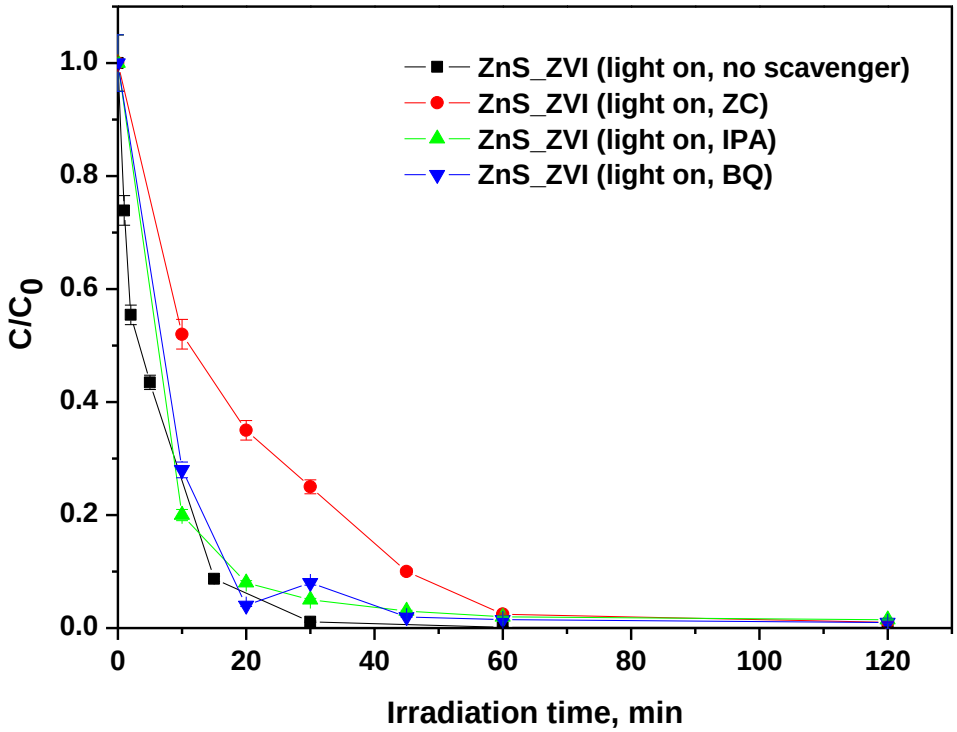

380

381 **Figure 7.** Effects of different scavengers on EBT degradation using ZnS_ZVI composite under

382 UV light.

383

384 In details, the addition of IPA and BQ does not influence the catalytic performances, indicating

385 that hydroxyl radicals and superoxide are not the active species responsible of the EBT

386 degradation process. The results achieved in presence of BQ can be explained considering that

387 the reduction potential of O_2 to superoxide (E_0=-0.33 eV vs. NHE [56]) is less negative than

388 Fe^{2+}/Fe^0 reduction potential (E_0=−0.44 eV vs. NHE). Therefore, it is possible to argue that the

389 electrons on the CB of ZnS preferentially reduce Fe^{2+} to Fe^0 instead to reduce O_2 to superoxide.

390 The results achieved in presence of IPA prove that hydroxyl radicals do not participate in the

391 transformation of EBT molecules into the degradation products since the activity is similar to

that observed in the absence of scavengers. On the other hand, the TOC measured after 180 min of run time in presence of IPA was about 20 %, significantly lower than that obtained without the addition of IPA in the reaction medium (about 45 %). This result clearly evidences that hydroxyl radicals are the main reactive species involved in the mineralization of the degradation products generated by the reaction of EBT with Fe^0 in the ZnS_ZVI composite.

Finally, from the observation of the results achieved in presence of ZC, it is evident that electrons play a significant role in EBT degradation due to the decrease in the dye degradation efficiency, as shown in Figure 6. These last results clearly demonstrate that the high activity of ZnS_ZVI composite under UV light is linked to the capacity of electrons promoted in CB of ZnS in reducing Fe^{2+} (generated from the reaction reported in the Scheme 1) to Fe^0.

In summary, the mechanism of UV light assisted EBT degradation in presence of the ZnS_ZVI composite could be schematized with the following simplified reactions:

$ZnS + h\nu \rightarrow e^- + h^+$ Eq. 4

$H_2O = H^+ + OH^-$ Eq. 5

$h^+ + OH^- \rightarrow \cdot OH$ Eq. 6

$EBT + 2Fe^0 + 4H^+ \rightarrow R–NH_2 + R'\text{-}NH_2 + 2Fe^{2+}$ Eq. 7

$EBT + Fe^{2+} \rightarrow Fe^{2+}\text{-}EBT$ Eq. 8

$R\text{-}NH_2 + R'\text{-}NH_2 + Fe^{2+}\text{-}EBT + \cdot OH \rightarrow$ oxidation products $+Fe^{2+}$ Eq. 9

$Fe^{2+} + 2e^- \rightarrow Fe^0$ Eq. 10

EBT molecules react with Fe^0 and H^+ (Eq. 7) forming hydrogenated compounds with

naphthalene ring ($R–NH_2$ and $R'-NH_2$) and Fe^{2+}, which in turn reacts with EBT forming Fe^{2+}-EBT complex (Eq. 8). Simultaneously, under UV light irradiation, electrons jump from VB to CB of ZnS and the h^+ produced into ZnS VB (Eq. 4) generate ·OH, which oxidize $R–NH_2$ and $R'-NH_2$ (Eq. 9), giving intermediate byproducts and possibly continue the oxidative degradation action until mineralization. ·OH also oxidizes the organic structure of Fe^{2+}-EBT complex (Eq. 9) forming Fe^{2+} and other oxidation products, as reported in a literature paper dealing with the degradation of Fe^{2+}-formic acid complex [57]. After the degradation of Fe^{2+}-EBT complex, Fe^{2+} turns back to the catalyst surface [57] and ZnS CB electrons (e^-) reduce Fe^{2+} to Fe^0 (Eq. 10), which therefore reacts with EBT molecules, starting again the azo bond cleavage reaction (Eq. 7). On the other hand it is not possible to exclude the formation of H_2O_2 in the absence of UV light through the oxidation of ZVI by O_2 present in the aqueous medium. This reaction produces also Fe^{2+} that in turns produce hydroxyl radicals by reacting with generated H_2O_2 [58]. The so formed hydroxyl radicals may contribute to EBT discoloration and/or mineralization. To have evidence of this possible behavior, additional degradation tests were performed in the absence of UV light using ZnS_ZVI composite under anaerobic (by bubbling N_2 in the aqueous solution) and aerobic (by bubbling air in the reaction medium) conditions. The obtained results showed that no difference in EBT discoloration and TOC removal was observed under both conditions, underlining that the –N=N– group reduction step followed the same mechanism in these different media. This result underlines that H_2O_2 is not involved in the degradation mechanism, consistently with literature dealing with azo dyes degradation by ZVI [59]. Additionally, no TOC removal was achieved in both cases because of the reaction between Fe^{2+} and EBT forming the Fe^{2+}-EBT complex (Scheme 2).

Therefore, we believe that the ZnS_ZVI composite combines very effectively the ZVI high

435 degradation ability to cleavage azo bond (-N=N-) with the ZnS photocatalytic ability in the
436 degradation of by-products generated from the reaction between EBT and ZVI.

437 *3.3 Degradation of PhCl using ZnS and ZnS_ZVI in presence of UV light irradiation*

438 The degradation effectiveness and reusability efficiency of the ZnS_ZVI composite was
439 investigated also towards a chlorinated aromatic solvent, chlorobenzene (PhCl), which is very
440 persistent in the environment and is reported in EPA lists as priority pollutants. The
441 decontamination from PhCl is particularly desirable as it pollutes the water during the production
442 of phenol, dinitrochlorobenzene, dynamite and intermediate products for dyes as well as
443 medicine [60, 61]. One commonly adopted solution for the dechlorination of chlorinated organic
444 solvents as PhCl is the use of ZVI particles [62]. However, the main disadvantages of using ZVI
445 particles for water decontamination are related to the easy iron oxidation and the resulting
446 surface passivation due to iron oxides formation that considerably reduce the system reactivity
447 [63]. To demonstrate that the ZnS_ZVI composite overcomes these ZVI limitations, PhCl
448 aqueous solutions were treated with ZnS_ZVI particles under UV light irradiation. The
449 dechlorination reaction (which implies the degradation of PhCl molecules) was carried out using
450 75 mL of PhCl solution with an initial concentration of 50 mg L^{-1} and a composite dosage of 0.6
451 $g \cdot L^{-1}$.

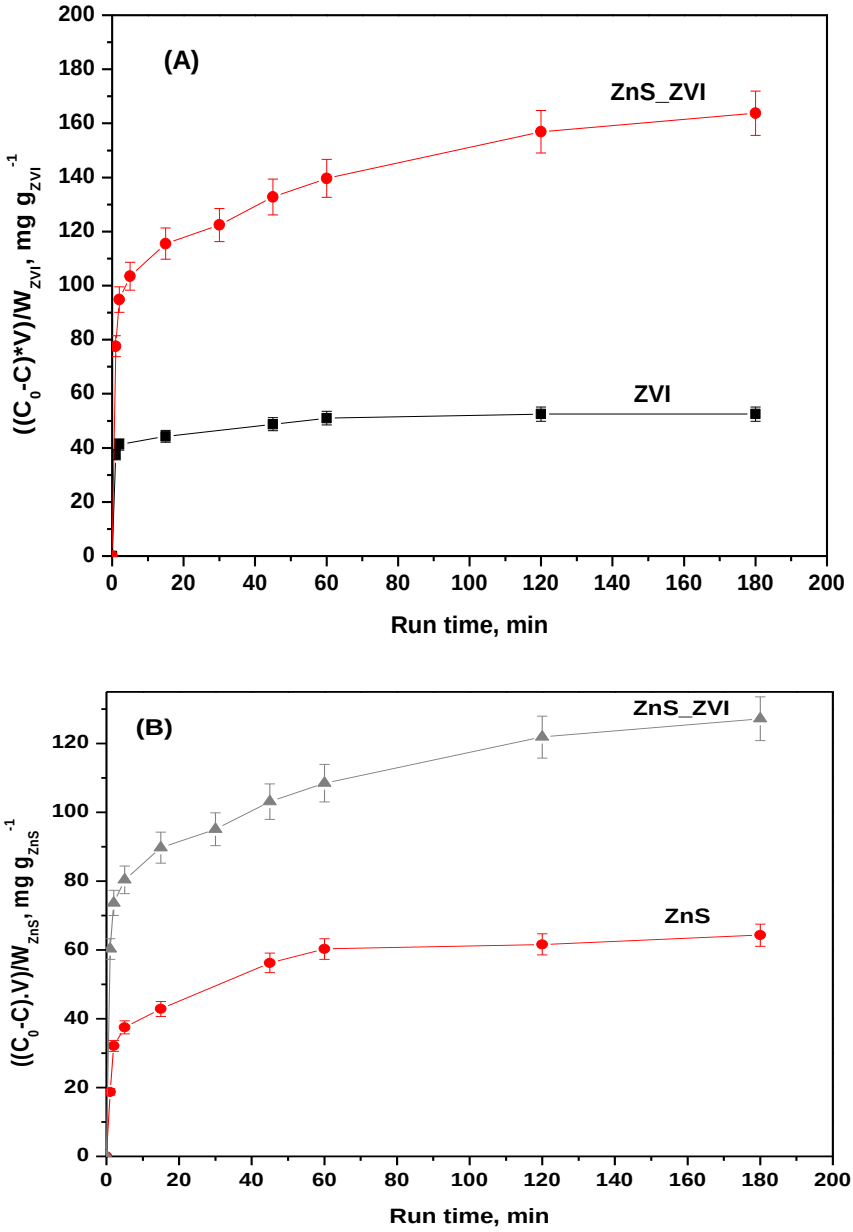

452 **Figure 8.** PhCl degradation under UV light irradiation using ZVI and ZnS_ZVI normalized with
453 respect to ZVI amount (A) and normalized with respect to ZnS amount (B) (C_0=initial PhCl
454 concentration, mg L^{-1}; V= volume of solution, L; W_{ZVI}= amount of ZVI, g; W_{ZnS}= amount of
455 ZnS, g).

456

457 Figure 8 shows the PhCl degradation activity of ZVI, ZnS and ZnS_ZVI. The reactivity of ZVI
458 and ZnS_ZVI, normalized with respect to ZVI amount in the composite, is compared in Figure
459 6A. The reactivity of ZnS and ZnS_ZVI, normalized with respect to ZnS amount in the
460 composite, is instead compared in Figure 6B. The PhCl degradation by using ZVI (Figure 8A,
461 bottom curve) is not very efficient, reaching a stationary value after 120 min of operating time,
462 while, as previously observed for EBT degradation, ZnS_ZVI composite under UV light
463 irradiation (Figure 8A, top curve) has a progressive reactivity increase over time, achieving, after
464 180 min, a value of about 160 mg g_{ZVI}^{-1} corresponding to the almost total degradation of PhCl
465 present in solution.
466 Similar behavior is obtained normalizing the results of PhCl degradation by using ZnS_ZVI with
467 respect the ZnS content in the composite (Figure 8B). In detail, ZnS_ZVI shows reactivity higher
468 (about double) than ZnS alone under UV irradiation. Additionally, a photolysis test (in presence
469 of only UV irradiation), carried out to check the stability of the target molecules in the used
470 operating conditions, evidenced a negligible PhCl degradation (about 1 %) in 180 min of run
471 time (data not shown).
472 Therefore, the better performances of ZnS_ZVI sample compared to ZVI and ZnS can be
473 explained by considering a synergic action between ZVI and ZnS in the composite, and not to
474 the simple mixing of the degradation properties related to only ZnS and ZVI.
475
476 *3.3.1 Reusability of ZnS_ZVI composite*
477 The reusability/recycling efficiency of ZnS_ZVI compared to that of ZVI was also evaluated for
478 the PhCl degradation process (Figure 9).

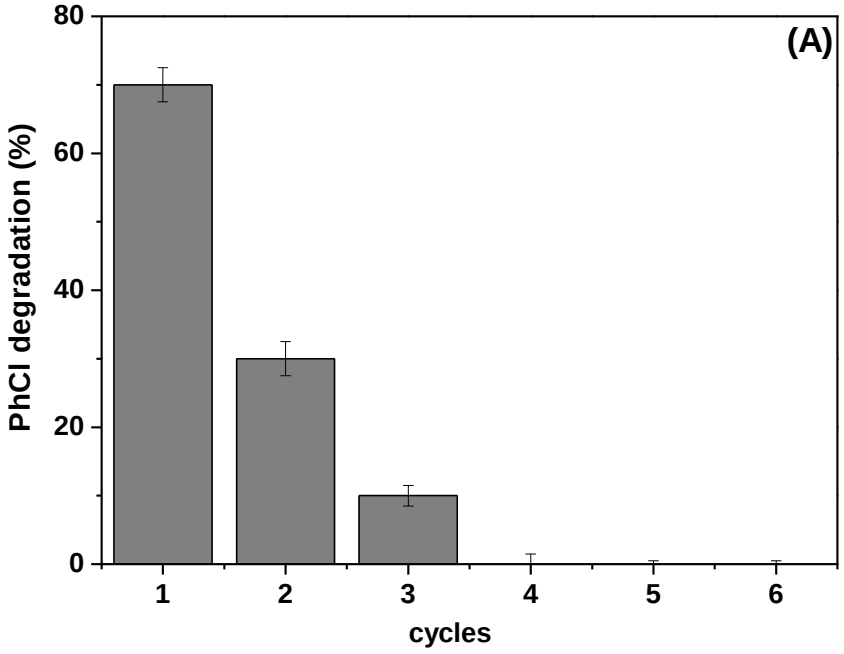
(A)
PhCl degradation (%)
0
20
40
60
80
1
2
3
4
5
6
cycles

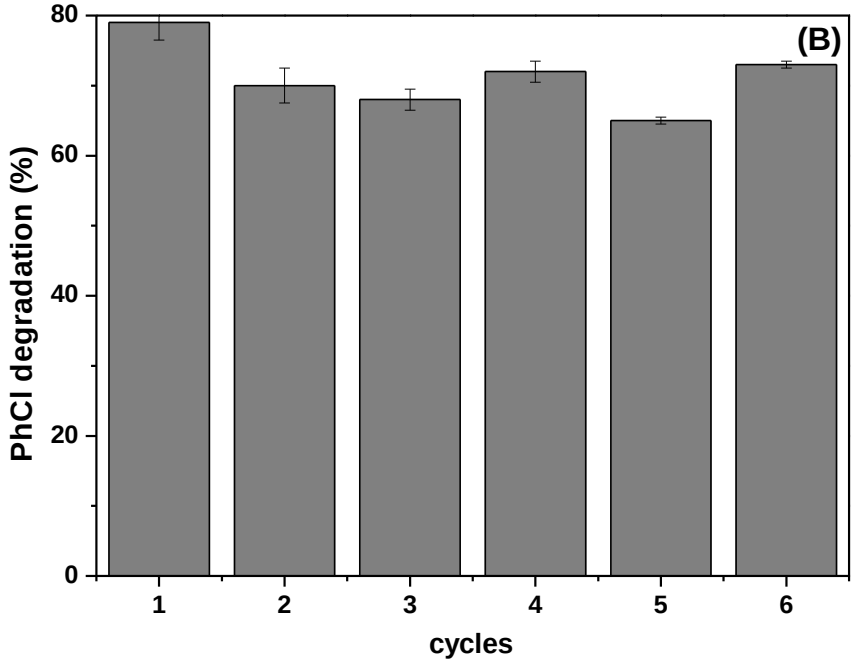
(B)
PhCl degradation (%)
0
20
40
60
80
1
2
3
4
5
6
cycles

Figure 9. Reuse cycles of unsupported ZVI (A) and UV irradiated ZnS_ZVI (B) on the PhCl degradation, after 60 min of operating time

Dechlorination capacity of unsupported ZVI (Figure 7A) is observed only for three cycles, showing a very rapid reactivity decay of the ZVI particles, as previously reported in literature [11]. Conversely, the PhCl degradation capacity of the ZnS_ZVI composite under UV light irradiation (Figure 7B) remains substantially constant, at the average value of 75 %, for all the reuse cycles.

The results of these tests, combined with those performed on EBT (Figure 4), undoubtedly demonstrate that the ZVI coupled to the ZnS photocatalyst, when irradiated by UV light, is able to maintain its high reactivity even after several reuse cycles.

4. Conclusions

In this work, ZnS semiconductor was coupled with zero-valent iron (ZVI) in order to achieve a composite (ZnS_ZVI) able to remove azo dyes and chlorinated organic pollutants from water avoiding the iron oxidative corrosion phenomena.

The activity properties were evaluated in the removal of eriochrome black T-dye (EBT) and chlorobenzene (PhCl) from aqueous solutions in presence of UV light.

The results demonstrated that under UV light irradiation, the almost total EBT and PhCl degradation were achieved after 30 min of treatment time for EBT and after 180 min for PhCl. ZnS_ZVI composite showed also enhanced catalytic properties compared to bare ZnS and unsupported ZVI. In detail, under UV light, ZnS_ZVI is able to reduce Fe^{2+} to Fe^{0} by the electrons promoted in the conduction band of ZnS, whereas the holes generated in the ZnS valence band lead to formation of hydroxyl radicals, which are able to further oxidize the intermediates generated from the reaction between the target pollutant and ZVI supported on

ZnS surface. ·OH formation was also confirmed by photoluminescence tests using terephthalic acid as a chemical probe. Furthermore, as regards the EBT degradation, the formation of a Fe^{2+}-EBT complex has been hypothesized and its structure was also suggested. Finally, a possible EBT degradation mechanism was also proposed.

Consecutive tests carried out on EBT or PhCl aqueous solutions using the same experimental conditions and without any regeneration steps, showed a complete reusability and high stability of the catalytic composite system, clearly proving that the simultaneous presence of UV light and ZnS lengthens the life cycle of ZVI, assuring its high reactivity also after several reuse cycles. Overall, the results reported in this paper clearly establish that the achieved ZnS_ZVI system is able to exploit the usual ZVI degradative capacities and, at the same time, makes ZVI recyclable when the catalytic system is continuously irradiated by UV light.

Acknowledgements

Financial support (PON FESR 2014-2020 ARS01-01398-INPOS, PON FESR 2014-2020 -RIS3 and PRIN 2015) of Ministero dell'Istruzione, dell'Università e della Ricerca (MIUR) is gratefully acknowledged. The authors wish to thank Maria Grazia Napoli, Ivano Immediata, Patrizia Iannece and Veronica Orlando for the technical support in chemical analysis

REFERENCES

[1] E. Petala, M. Baikousi, M.A. Karakassides, G. Zoppellaro, J. Filip, J. Tuček, K.C. Vasilopoulos, J. Pechoušek, R. Zbořil, Synthesis, physical properties and application of the zero-valent iron/titanium dioxide heterocomposite having high activity for the sustainable photocatalytic removal of hexavalent chromium in water, Physical Chemistry Chemical Physics, 18 (2016) 10637-10646.
[2] H.-J. Lu, J.-K. Wang, S. Ferguson, T. Wang, Y. Bao, H.-x. Hao, Mechanism, synthesis and modification of nano zerovalent iron in water treatment, Nanoscale, 8 (2016) 9962-9975.
[3] T. Pasinszki, M. Krebsz, Synthesis and Application of Zero-Valent Iron Nanoparticles in Water Treatment, Environmental Remediation, Catalysis, and Their Biological Effects, Nanomaterials, 10 (2020) 917.

[4] W. Shen, X. Wang, F. Jia, Z. Tong, H. Sun, X. Wang, F. Song, Z. Ai, L. Zhang, B. Chai, Amorphization enables highly efficient anaerobic thiamphenicol reduction by zero-valent iron, Applied Catalysis B: Environmental, 264 (2020) 118550.
[5] W. Xu, Z. Li, S. Shi, J. Qi, S. Cai, Y. Yu, D.M. O'Carroll, F. He, Carboxymethyl cellulose stabilized and sulfidated nanoscale zero-valent iron: Characterization and trichloroethene dechlorination, Applied Catalysis B: Environmental, 262 (2020) 118303.
[6] C.J. Lin, S.L. Lo, Y.H. Liou, Dechlorination of trichloroethylene in aqueous solution by noble metal-modified iron, Journal of hazardous materials, 116 (2004) 219-228.
[7] Y. Gao, F. Wang, Y. Wu, R. Naidu, Z. Chen, Comparison of degradation mechanisms of microcystin-LR using nanoscale zero-valent iron (nZVI) and bimetallic Fe/Ni and Fe/Pd nanoparticles, Chemical engineering journal, 285 (2016) 459-466.
[8] A.D. Bokare, R.C. Chikate, C.V. Rode, K.M. Paknikar, Effect of surface chemistry of Fe− Ni nanoparticles on mechanistic pathways of azo dye degradation, Environmental science & technology, 41 (2007) 7437-7443.
[9] C.-Y. Hu, S.-L. Lo, Y.-H. Liou, Y.-W. Hsu, K. Shih, C.-J. Lin, Hexavalent chromium removal from near natural water by copper–iron bimetallic particles, Water Research, 44 (2010) 3101-3108.
[10] Y. Liu, J. Wang, Reduction of nitrate by zero valent iron (ZVI)-based materials: A review, Science of The Total Environment, 671 (2019) 388-403.
[11] C. Huang, W.-P. Hsieh, J.R. Pan, S.-M. Chang, Characteristic of an innovative TiO2/Fe0 composite for treatment of azo dye, Separation and Purification Technology, 58 (2007) 152-158.
[12] K. Kobwittaya, S. Sirivithayapakorn, Photocatalytic reduction of nitrate over Fe-modified TiO2, ScienceDirect. APCBEE Procedia, 10 (2014) 321-325.
[13] A. KHANI, M.R. SOHRABI, M. KHOSRAVI, M. DAVALLO, Enhancing purification of an azo dye solution in nanosized zero-valent iron-ZnO photocatalyst system using subsequent semibatch packed-bed reactor, Turkish Journal of Engineering and Environmental Sciences, 37 (2013) 91-99.
[14] X. Wang, M. Hong, F. Zhang, Z. Zhuang, Y. Yu, Recyclable nanoscale zero valent iron doped g-C3N4/MoS2 for efficient photocatalysis of RhB and Cr (VI) driven by visible light, ACS Sustainable Chemistry & Engineering, 4 (2016) 4055-4063.
[15] X. Wang, D. Lizong, Well-dispersed zero-valent iron supported on Fe 3 O 4/gC 3 N 4 composites via a facile approach with versatile photoredox catalysis, Journal of Nanoparticle Research, 20 (2018) 317.
[16] O. Sacco, V. Vaiano, C. Daniel, W. Navarra, V. Venditto, Highly robust and selective system for water pollutants removal: How to transform a traditional photocatalyst into a highly robust and selective system for water pollutants removal, Nanomaterials, 9 (2019).
[17] V. Vaiano, O. Sacco, D. Sannino, Electric energy saving in photocatalytic removal of crystal violet dye through the simultaneous use of long-persistent blue phosphors, nitrogen-doped TiO2 and UV-light emitting diodes, Journal of Cleaner Production, 210 (2019) 1015-1021.
[18] N. Fessi, M.F. Nsib, Y. Chevalier, C. Guillard, F. Dappozze, A. Houas, L. Palmisano, F. Parrino, Photocatalytic degradation enhancement in pickering emulsions stabilized by solid particles of bare TiO 2, Langmuir, 35 (2019) 2129-2136.
[19] M. Bellardita, C. Garlisi, A.M. Venezia, G. Palmisano, L. Palmisano, Influence of fluorine on the synthesis of anatase TiO2 for photocatalytic partial oxidation: Are exposed facets the main actors?, Catalysis Science and Technology, 8 (2018) 1606-1620.

[20] T. Montini, V. Gombac, A. Hameed, L. Felisari, G. Adami, P. Fornasiero, Synthesis, characterization and photocatalytic performance of transition metal tungstates, Chemical Physics Letters, 498 (2010) 113-119.
[21] X. Chen, Y. Zhou, Q. Liu, Z. Li, J. Liu, Z. Zou, Ultrathin, single-crystal WO3 nanosheets by two-dimensional oriented attachment toward enhanced photocatalystic reduction of CO2 into hydrocarbon fuels under visible light, ACS applied materials & interfaces, 4 (2012) 3372-3377.
[22] O. Sacco, J. Murcia, A. Lara, M. Hernández-Laverde, H. Rojas, J. Navío, M. Hidalgo, V. Vaiano, Pt–TiO2–Nb2O5 heterojunction as effective photocatalyst for the degradation of diclofenac and ketoprofen, Materials Science in Semiconductor Processing, 107 (2020) 104839.
[23] S. Mofokeng, V. Kumar, R. Kroon, O. Ntwaeaborwa, Structure and optical properties of Dy3+ activated sol-gel ZnO-TiO2 nanocomposites, Journal of Alloys and Compounds, 711 (2017) 121-131.
[24] F.A. Chowdhury, Z. Mi, M.G. Kibria, M.L. Trudeau, Group III-nitride nanowire structures for photocatalytic hydrogen evolution under visible light irradiation, APL Materials, 3 (2015) 104408.
[25] O. Sacco, V. Vaiano, D. Sannino, R.A. Picca, N. Cioffi, Ag modified ZnS for photocatalytic water pollutants degradation: Influence of metal loading and preparation method, Journal of Colloid and Interface Science, 537 (2019) 671-681.
[26] Y. Zhang, Z. Jin, H. Yuan, G. Wang, B. Ma, Well-regulated nickel nanoparticles functional modified ZIF-67 (Co) derived Co3O4/CdS pn heterojunction for efficient photocatalytic hydrogen evolution, Applied Surface Science, 462 (2018) 213-225.
[27] J. Luo, X. Zhou, X. Ning, L. Zhan, J. Chen, Z. Li, Constructing a direct Z-scheme La2NiO4/g-C3N4 hybrid photocatalyst with boosted visible light photocatalytic activity, Separation and Purification Technology, 201 (2018) 327-335.
[28] D. Friedmann, A. Hakki, H. Kim, W. Choi, D. Bahnemann, Heterogeneous photocatalytic organic synthesis: state-of-the-art and future perspectives, Green Chemistry, 18 (2016) 5391-5411.
[29] S. Anandan, Y. Ikuma, K. Niwa, An overview of semi-conductor photocatalysis: modification of TiO2 nanomaterials, in: Solid State Phenomena, Trans Tech Publ, 2010, pp. 239-260.
[30] H. Liu, T. Chen, Q. Xie, X. Zou, C. Chen, R.L. Frost, The functionalization of limonite to prepare NZVI and its application in decomposition of p-nitrophenol, Journal of Nanoparticle Research, 17 (2015) 374.
[31] J.M. Yan, X.B. Zhang, S. Han, H. Shioyama, Q. Xu, Iron-nanoparticle-catalyzed hydrolytic dehydrogenation of ammonia borane for chemical hydrogen storage, Angewandte Chemie, 120 (2008) 2319-2321.
[32] W.N. O. Sacco, V. Vaiano, V. Venditto, C. Daniel, Rapid degradation of p-nitrophenol in aqueous solution by novel photocatalyst based on zero-valent iron 11th European Conference on Solar Chemistry and Photocatalysis: Environmental Applications (SPEA) (submitted), (2020).
[33] V. Vaiano, O. Sacco, D. Sannino, Enhanced photocatalytic degradation of organic pollutants in wastewater using photocatalysts coupled with luminescent materials, Chemical Engineering Transactions, 60 (2017) 211-216.
[34] S.K. Kansal, S. Sood, A. Umar, S. Mehta, Photocatalytic degradation of Eriochrome Black T dye using well-crystalline anatase TiO2 nanoparticles, Journal of Alloys and Compounds, 581 (2013) 392-397.

620 [35] A. Mishra, A. Mehta, M. Sharma, S. Basu, Impact of Ag nanoparticles on
621 photomineralization of chlorobenzene by TiO2/bentonite nanocomposite, Journal of
622 environmental chemical engineering, 5 (2017) 644-651.
623 [36] P. Franco, O. Sacco, I. De Marco, D. Sannino, V. Vaiano, Photocatalytic Degradation of
624 Eriochrome Black-T Azo Dye Using Eu-Doped ZnO Prepared by Supercritical Antisolvent
625 Precipitation Route: A Preliminary Investigation, Topics in Catalysis, 63 (2020) 1193-1205.
626 [37] Y. Son, V. Mishin, W. Welsh, S.-E. Lu, J.D. Laskin, H. Kipen, Q. Meng, A novel high-
627 throughput approach to measure hydroxyl radicals induced by airborne particulate matter,
628 International journal of environmental research and public health, 12 (2015) 13678-13695.
629 [38] N. Mehrotra, R.M. Tripathi, F. Zafar, M.P. Singh, Catalytic degradation of dichlorvos using
630 biosynthesized zero valent iron nanoparticles, IEEE Transactions on NanoBioscience, 16 (2017)
631 280-286.
632 [39] A. Fairbrother, V. Izquierdo-Roca, X. Fontané, M. Ibáñez, A. Cabot, E. Saucedo, A. Pérez-
633 Rodríguez, ZnS grain size effects on near-resonant Raman scattering: optical non-destructive
634 grain size estimation, CrystEngComm, 16 (2014) 4120-4125.
635 [40] X. Guan, Y. Sun, H. Qin, J. Li, I.M. Lo, D. He, H. Dong, The limitations of applying zero-
636 valent iron technology in contaminants sequestration and the corresponding countermeasures: the
637 development in zero-valent iron technology in the last two decades (1994–2014), Water research,
638 75 (2015) 224-248.
639 [41] J. Cao, L. Wei, Q. Huang, L. Wang, S. Han, Reducing degradation of azo dye by zero-
640 valent iron in aqueous solution, chemosphere, 38 (1999) 565-571.
641 [42] E.C. Lumbaque, M.F. Gomes, V.D.S. Carvalho, A.M. de Freitas, E.R.L. Tiburtius,
642 Degradation and ecotoxicity of dye Reactive Black 5 after reductive-oxidative process,
643 Environmental Science and Pollution Research, 24 (2017) 6126-6134.
644 [43] S. Dutta, R. Saha, H. Kalita, A.N. Bezbaruah, Rapid reductive degradation of azo and
645 anthraquinone dyes by nanoscale zero-valent iron, Environmental Technology & Innovation, 5
646 (2016) 176-187.
647 [44] N. Srivastava, M. Shukla, S. Saha, An unusual way to synthesize 1-nitronaphthalene from 1-
648 amino-5-nitronaphthalene, African Journal of Pharmacy and Pharmacology, 5 (2011) 542-546.
649 [45] H. Hodgson, D. Hathway, The absorption spectra of some mono-nitronaphthylamines, with
650 observations on their structures, Transactions of the Faraday Society, 41 (1945) 115-121.
651 [46] Y. Zhang, F. Gao, B. Wanjala, Z. Li, G. Cernigliaro, Z. Gu, High efficiency reductive
652 degradation of a wide range of azo dyes by SiO2-Co core-shell nanoparticles, Applied Catalysis
653 B: Environmental, 199 (2016) 504-513.
654 [47] W. Feng, D. Nansheng, H. Helin, Degradation mechanism of azo dye CI reactive red 2 by
655 iron powder reduction and photooxidation in aqueous solutions, Chemosphere, 41 (2000) 1233-
656 1238.
657 [48] H. Zhang, Y. Ruan, A. Liang, K. Shih, Z. Diao, M. Su, D. Chen, H. Lu, L. Kong,
658 Carbothermal reduction for preparing nZVI/BC to extract uranium: insight into the iron species
659 dependent uranium adsorption behavior, Journal of Cleaner Production, 239 (2019) 117873.
660 [49] O. Kruglaya, L. Zakharkin, B. Petrov, G. Kalinina, N. Vyazankin, Synthesis and Reactivity
661 in Inorganic and Metal-Organic Chemistry, Inorganic and Nano-Metal Chemistry, 3 (1973) 63-
662 73.
663 [50] A.J. Dos Santos, M.D. De Lima, D.R. Da Silva, S. Garcia-Segura, C.A. Martínez-Huitle,
664 Influence of the water hardness on the performance of electro-Fenton approach: decolorization
665 and mineralization of Eriochrome Black T, Electrochimica Acta, 208 (2016) 156-163.

[51] Á.R.L. da Silva, A.J. dos Santos, E.V. dos Santos, D.R. da Silva, C.A. Martínez-Huitle, Theoretical and experimental study of the influence of cation–Eriochrome complexes on the BDD anodic oxidation of Eriochrome Black T solutions, Electrochemistry Communications, 112 (2020) 106668.
[52] G. Pandey, Fe–EBT Chelate Complex: A Novel Mean for Growth of α-FeOOH and γ-Fe 2 O 3 Nanostructures, Acta Metallurgica Sinica (English Letters), 27 (2014) 1127-1133.
[53] Y. Zhong, K. Shih, Z. Diao, G. Song, M. Su, D. Chen, L. Kong, Peroxymonosulfate activation through LED-induced ZnFe2O4 for levofloxacin degradation, Chemical Engineering Journal, 417 (2021) 129225.
[54] A. Mancuso, O. Sacco, D. Sannino, S. Pragliola, V. Vaiano, Enhanced visible-light-driven photodegradation of Acid Orange 7 azo dye in aqueous solution using Fe-N co-doped TiO2, Arabian Journal of Chemistry, 13 (2020) 8347-8360.
[55] A. Raevskaya, A. Korzhak, A. Stroyuk, S.Y. Kuchmii, Photocatalytic reduction of Zn (II) with participation of ZnS nanoparticles, Theoretical and Experimental Chemistry, 41 (2005) 241-246.
[56] P.M. Wood, The redox potential of the system oxygen—superoxide, Febs Letters, 44 (1974) 22-24.
[57] J. Arana, O.G. Dıaz, M.M. Saracho, J.D. Rodrıguez, J.H. Melián, J.P. Peña, Photocatalytic degradation of formic acid using Fe/TiO2 catalysts: the role of Fe3+/Fe2+ ions in the degradation mechanism, Applied Catalysis B: Environmental, 32 (2001) 49-61.
[58] J. Yao, Y. Yu, R. Qu, J. Chen, Z. Huo, F. Zhu, Z. Wang, Fe-Activated Peroxymonosulfate Enhances the Degradation of Dibutyl Phthalate on Ground Quartz Sand, Environmental Science & Technology, 54 (2020) 9052-9061.
[59] W.S. Pereira, R.S. Freire, Azo dye degradation by recycled waste zero-valent iron powder, Journal of the Brazilian Chemical Society, 17 (2006) 832-838.
[60] Y. Liu, X. Jiang, Plasma-induced degradation of chlorobenzene in aqueous solution, Plasma Chemistry and Plasma Processing, 28 (2008) 15-24.
[61] W.-x. Zhang, C.-B. Wang, H.-L. Lien, Treatment of chlorinated organic contaminants with nanoscale bimetallic particles, Catalysis today, 40 (1998) 387-395.
[62] C.L. Lee, C.J.G. Jou, H.P. Wang, Enhanced Degradation of Chlorobenzene in Aqueous Solution Using Microwave-Induced Zero-Valent Iron and Copper Particles, Water environment research, 82 (2010) 642-647.
[63] Y. Pang, Y. Ruan, Y. Feng, Z. Diao, K. Shih, D. Chen, L. Kong, Ultrasound assisted zero valent iron corrosion for peroxymonosulfate activation for Rhodamine-B degradation, Chemosphere, 228 (2019) 412-417.